

Generative modeling through internal high-dimensional chaotic activity

Samantha J. Fournier^{1,*} and Pierfrancesco Urbani¹

¹*Université Paris Saclay, CNRS, CEA, Institut de physique théorique, F-91191 Gif-sur-Yvette, France*

Generative modeling aims at producing new datapoints whose statistical properties resemble the ones in a training dataset. In recent years, there has been a burst of machine learning techniques and settings that can achieve this goal with remarkable performances. In most of these settings, one uses the training dataset in conjunction with noise, which is added as a source of statistical variability and is essential for the generative task. Here, we explore the idea of using internal chaotic dynamics in high-dimensional chaotic systems as a way to generate new datapoints from a training dataset. We show that simple learning rules can achieve this goal within a set of vanilla architectures and characterize the quality of the generated datapoints through standard accuracy measures.

I. INTRODUCTION

Generative models aim to create samples statistically similar to those belonging to a training dataset: their goal is to fit the probability distribution from which the datapoints supposedly come from. In a generic setting, this probability distribution takes the form of a Boltzmann factor. The corresponding Energy Based Models (EBMs) fit the parameters of the Hamiltonian of the Boltzmann distribution and can be viewed as maximum entropy models, where the statistical properties of the dataset are imposed as constraints to low degree correlation functions [1, 2], (see [3, 4] for recent reviews). The resulting learning rule can be viewed as a gradient ascent on the Log-Likelihood (LL). However, running the training dynamics is a notoriously challenging task: at each epoch, the evaluation of the gradient of the LL requires the computation of the correlation functions of the degrees of freedom as predicted from the current estimation of the model’s probability distribution. This is typically an intractable problem from an analytical point of view and is generally tackled numerically through parallel Monte Carlo Markov Chain (MCMC) simulations. The main drawback of this strategy is that MCMC must be run for times that are larger than the mixing time, which can be very large especially in the low temperature phase and with datapoints clustered in high dimensions. Indeed in this case, the corresponding Boltzmann distributions are peaked on far-apart regions of phase space that are separated by free-energy barriers scaling with the dimension of the system. Exploring each of these regions requires activated dynamical trajectories, which implies that the MCMC is very slow to thermalize. Therefore, training EBMs requires so much computational effort that—in practice—the corresponding MCMC is never thermalized and the gradient ascent on the LL is performed in an out-of-equilibrium fashion, with only a few Monte Carlo steps.

A first approximate solution to this problem was proposed using clever initializations of the MCMCs [5, 6]. However, recent works [7, 8] have shown that Restricted Boltzmann Machines (RBMs)—a particular class of EBMs—trained with short-run, randomly initialized MCMCs can still generate good-looking samples, provided that the schedule for the generation process coincides with the one used during the training dynamics. Therefore in these (extreme) experiments, the learning dynamics is not supposed to use a proxy for the exact gradient of the LL since the MCMC never gets to equilibrium. Correspondingly, the training trajectory is not maximizing the LL and yet the trained RBMs can generate good-looking samples.

These results can be reformulated by replacing the MCMC sampling dynamics with the following Langevin algorithm. Calling $-E$ the LL, one can replace MCMC with

$$\frac{d\mathbf{x}}{dt} = -\frac{\partial E}{\partial \mathbf{x}} + \boldsymbol{\eta}(t) \quad (1)$$

where $\boldsymbol{\eta}$ is just white noise and \mathbf{x} are the dynamical degrees of freedom of which one would like to know specific correlation functions. The stationary probability distribution of eq. (1) is the model’s Boltzmann measure with energy E . However, this stationary measure is attained only asymptotically and the results of [7, 8] showed that it is not necessary to wait for such long times: sampling the stochastic trajectories properly (i.e. with random initializations) on finite time windows and fitting according to the model’s parameters, one can get an effective generative model. Therefore in this case, the system in (1) is held out-of-equilibrium in the sense that configurations are sampled before reaching the Boltzmann distribution. The question we are interested in in this work concerns how we can generalize the out-of-equilibrium dynamics and noise that can be used to generate new samples. This question is very broad

* Correspondence email address: samantha.fournier@ipht.fr

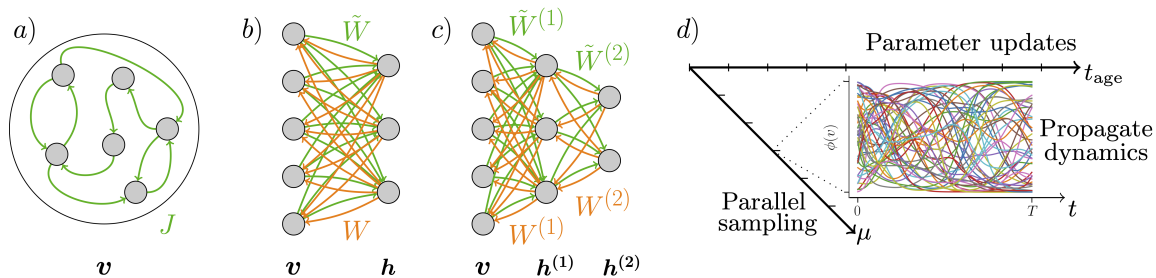


Figure 1. The three different architectures considered in this work: a) Unrestricted architecture, b) Restricted 2-layer architecture and c) Restricted 3-layer architecture. The fields \mathbf{b} , \mathbf{c} and \mathbf{d} are not represented. Panel d): Pipeline of training protocol.

and here we focus on the particular case in which the out-of-equilibrium dynamics is represented by a chaotic, high-dimensional activity induced by recurrent connections in the architecture of the generative models. Our interest in this particular setting is related to neuroscience questions: we would like to try to understand if it is possible to train recurrent neural networks as generative models. In the following, we define a set of models and training algorithms with this purpose and present evidence that we can achieve via recurrent architectures good generative performances that we carefully quantify with standard accuracy indices.

II. DEFINITION OF THE MODELS

In what follows, we consider the setting in which we have a training dataset $\mathcal{D} = \{\xi^{(\mu)}\}_{\mu=1, \dots, N_s}$ composed by N_s points which are N_v -dimensional vectors ξ^μ and the generative task is to produce new datapoints that are statistically equivalent to the ones contained in the dataset. The models we are going to define belong to a general class of dynamical systems which are high-dimensional and chaotic. We consider three architectures whose recurrent and asymmetric connections are used to produce chaotic dynamics which can be used for generative purposes. The parameters of the different models are trained with rules adapted from the usual contrastive Hebbian learning algorithms [9], where we replace the parallel MCMC sampling by parallel simulations of the dynamical system under study. The resulting generative models are straightforward to train and more biologically plausible than standard EBMs because they do not require the injection of noise by an external operator.

Unrestricted architecture – We consider one layer of N_v variables $\mathbf{v} = \{v_i\}_{i=1, \dots, N_v}$ that are recurrently connected. They evolve according to

$$\tau \frac{dv_i}{dt} = -v_i + \frac{1}{\sqrt{N_v}} \sum_{j=1}^{N_v} (J_{ij} + A_{ij}) \phi(v_j) + b_i \quad (2)$$

where $\phi(\cdot) = \tanh(\cdot)$ is a non-linear activation function and τ fixes an intrinsic timescale in the dynamics. The matrix J is random with Gaussian independent entries with zero mean and variance g . We use g as a control parameter: if g is sufficiently large, the dynamical system with $A_{ij} = 0$ and $b_i = 0$ is in a chaotic phase [10]. Therefore, the matrix J will be used as a source of chaotic activity that drives the generative dynamics. The matrix A and the field \mathbf{b} are instead parameters that we train via contrastive Hebbian learning. They are both initialized to zero and at each epoch t_{age} they are updated according to the rule

$$\begin{aligned} \Delta A_{ij} &= k (\langle \xi_i \xi_j \rangle_{\mathcal{D}} - \langle \phi(v_i) \phi(v_j) \rangle_{\mathcal{F}}) \\ \Delta b_i &= k (\langle \xi_i \rangle_{\mathcal{D}} - \langle \phi(v_i) \rangle_{\mathcal{F}}), \end{aligned} \quad (3)$$

where $\langle \cdot \rangle_{\mathcal{D}}$ is the empirical average over a minibatch of size M of the training dataset—changed at each training epoch—and $\langle \cdot \rangle_{\mathcal{F}}$ is an empirical average over a set of M configurations $\mathcal{F} = \{\phi(\mathbf{v}^{(\mu)})(T)\}_{\mu=1, \dots, M}$ collected by simulating the dynamical system (2) up to time T , starting from independent random initial conditions. The parameter k is the learning rate. Since the learning rule for A is symmetric, training will suppress chaos by planting fixed points into the dynamics. The goal of the generative dynamics is to find the optimal parameters A and \mathbf{b} that suppress chaos just enough to allow good generative performances.

Restricted architecture – In the context of EBMs, adding to the visible variables a set of latent variables allows to encode higher-order interactions in the former and this is a way of constructing more expressive generative models.

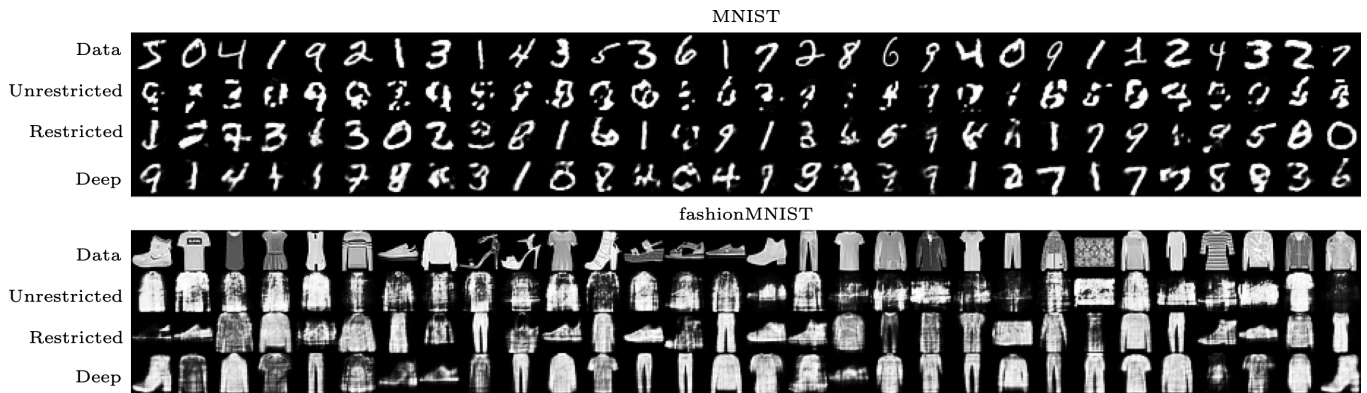


Figure 2. Data samples and generated samples from the trained models. Parameters: $N_v = 784$ (which is the dimension of each data sample), $N_h = N_h^{(1)} = 500$, $N_h^{(2)} = 100$, $dt = 1$, $\tau = 10$, $T = 100$, $g = 1.5$, $k = 0.01$, $M = 500$, $N_s = 10\,000$. Training lasted 300 000 epochs in all cases except for the Deep model trained on FashionMNIST where training lasted 400 000 epochs.

We adapt the standard architecture of RBMs [11] to construct a dynamical system composed of two layers of variables: the visible \mathbf{v} and hidden \mathbf{h} units, with no intra-layer connections. The variables are subjected to the dynamics

$$\tau \frac{dv_i}{dt} = -v_i + \frac{1}{\sqrt{N_h}} \sum_{a=1}^{N_h} (W_{ia} + A_{ia}) \phi(h_a) + b_i, \quad (5)$$

$$\tau \frac{dh_a}{dt} = -h_a + \frac{1}{\sqrt{N_v}} \sum_{i=1}^{N_v} (\tilde{W}_{ai} + A_{ai}) \phi(v_i) + c_a, \quad (6)$$

with $i = 1, \dots, N_v$ and $a = 1, \dots, N_h$. The matrix elements of the connections W , \tilde{W} are drawn at random from two Gaussian distributions with mean 0 and variance g . These matrices are fixed and the control parameter g tunes the level of chaos in the untrained network. The fields \mathbf{b} , \mathbf{c} and the symmetric connections A are parameters of the model that are initialized at zero and trained. The corresponding update rule, at each epoch t_{age} , is written as

$$\Delta A_{ia} = k (\langle \xi_i \chi_a \rangle_{\mathcal{D}} - \langle \phi(v_i) \phi(h_a) \rangle_{\mathcal{F}}) \quad (7)$$

$$\Delta b_i = k (\langle \xi_i \rangle_{\mathcal{D}} - \langle \phi(v_i) \rangle_{\mathcal{F}}) \quad (8)$$

$$\Delta c_a = k (\langle \chi_a \rangle_{\mathcal{D}} - \langle \phi(h_a) \rangle_{\mathcal{F}}), \quad (9)$$

where now the samples $\{\chi^{(\mu)}(T) = \phi(\mathbf{h}^{(\mu)}(T))\}_{\mu=1, \dots, M}$ are collected from simulating the hidden units' dynamics (6) up to time T , starting from independent random initial conditions, while the visible units are clamped $\phi(\mathbf{v}^{(\mu)})(t) = \boldsymbol{\xi}^{(\mu)}$ to a data sample. One advantage of not introducing intra-layer connections is that when the visible units are clamped, Eq. (6) can be integrated directly

$$\chi_a^{(\mu)}(T) = \chi_a^{(\mu)}(0) e^{-T/\tau} + \left(\frac{1}{\sqrt{N_v}} \sum_{i=1}^{N_v} (\tilde{W}_{ai} + A_{ai}) \xi_i^{(\mu)} + c_a \right) (1 - e^{-T/\tau}). \quad (10)$$

The crucial difference between the model considered here and standard RBM architectures is that here $\tilde{W} \neq W^T$ so the connections between layers are in general not symmetric. In the case of symmetric connections, one can see the dynamics in Eqs. (5)-(6) as some gradient descent on a carefully defined Lyapunov function [12]. In the asymmetric case instead, one expects chaotic activity [13], which can be used as a sort of generative noise.

Deep and restricted architecture – For the last architecture, we consider a generalization of the restricted one described above where we add an extra hidden layer to increase the depth of the model. This is introduced to capture more easily higher-order interactions between visible degrees of freedom. Therefore, we consider three layers of variables: \mathbf{v} , $\mathbf{h}^{(1)}$ and $\mathbf{h}^{(2)}$ —still with no intra-layer connections. The precise architecture is represented in Fig. 1-c. The equations of motion are generalizations of Eqs. (5)-(6) (see Appendix A for details). It must be noted that in this case the dynamics of the hidden neurons when the visible layer is clamped is not integrable and must be simulated as well.

Training protocol – The pipeline of training is summarized in Fig. 1-d and is the same for all the architectures considered. At each epoch t_{age} , M parallel simulations of the dynamical systems are run up to a target time T .

To this end, the dynamical equations are Euler discretized with a timestep dt . The initial values of all degrees of freedom $\mathbf{x} = \{\mathbf{v}, \mathbf{h}\}$ are extracted at random from a normal probability distribution. Their configurations at time T are collected in the set $\mathcal{F} = \{\phi(\mathbf{x}^{(\mu)})(T)\}_{\mu=1, \dots, M}$. These configurations are then used to compute the negative terms in the learning rules. Furthermore, the empirical averages over the dataset appearing in the positive terms of the learning rules are computed from a mini-batch also of size M of the training dataset. The parameters of the models are thus updated at each epoch t_{age} with a learning rate k . This training strategy is similar to what was done in [7, 8] where RBMs were trained using MCMCs initialized at random and simulated for order 10 to 100 Monte Carlo steps. To gain efficiency, the dynamics is implemented with PyTorch and run on a GPU.

III. RESULTS

We tested the proposed models on the MNIST [14, 15] and Fashion-MNIST [16] datasets, which are composed of grey images $\boldsymbol{\xi} \in [0, 255]^{N_v}$. Since the dynamical systems are read through an activation function ϕ whose output is bounded between -1 and 1, we trained our models on transformed data samples $\boldsymbol{\xi} \rightarrow f(\boldsymbol{\xi}) = 2\frac{\boldsymbol{\xi}}{255} - 1 \in [-1, 1]^{N_v}$, and then performed the inverse transform to plot the generated samples as grey images. The samples generated by the trained models can be found Fig. 2: they correspond to the activity of the visible layer \mathbf{v} at time T , starting from a random initialization. The 1-layer Unrestricted model generated samples that were recognizable but noisy overall. The 2- and 3-layers Restricted models generated samples that were qualitatively similar, and overall better than in the 1-layer case. While our motivation for the introduction of an additional layer to the Restricted model was to capture finer details of the data samples, we have seen that we did not get significant improvements in the quality of the generated samples. Nevertheless, the 3-layer architecture performed successfully, given that it was trained with vanilla learning rules and no special pre-training [17, 18].

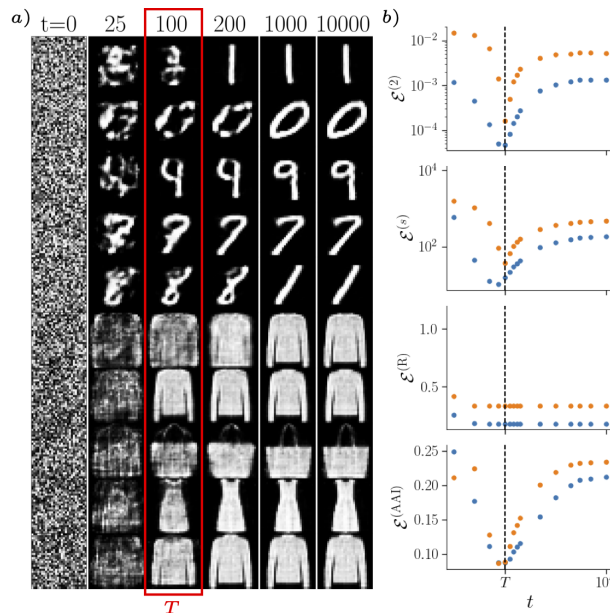


Figure 3. Panel *a*) Samples generated at different times t from the 2-layer Restricted model trained on MNIST (top half) and FashionMNIST (bottom half) with the same parameters as in Fig. 2. Panel *b*) Performance at different times t of the latter model trained on MNIST (blue dots) and FashionMNIST (orange dots) across 4 accuracy indices (see Appendix B for their definitions). The lower these indices are, the better the generated samples. All the accuracy indices are computed on a testing dataset composed of $N_s = 10\,000$ data samples.

In Fig. 3-a, we show some samples generated by the trained 2-layer Restricted model at different times t , starting from a random initialization at $t = 0$. During training, the dynamical system always learns a set of fixed-points that correspond to some "good" samples and that are reached for times $t > T$ (i.e. see the samples generated at $t > 1\,000$). These fixed-points attractors however are just a small fraction of the rich repertoire of samples that the trained models are able to generate. It is important to stress that the dynamics of the trained models at $t = T$ is chaotic: the system is wandering in a low-dimensional subspace surrounding the fixed-points attractors. In Fig. 3-b, the statistical quality of the samples generated by the trained model is assessed through standard accuracy indices. The peak in

performance at $t = T$ was observed in [8] for RBMs trained with short-run, randomly initialized MCMCs. We obtain similar values of $\mathcal{E}^{(2)}$ and $\mathcal{E}^{(AAI)}$ as Ref. [8] at peak performance for a comparable number of training epochs: see the *dark blue* curves in Fig. 3 of Ref. [8] Supplementary material, where the equivalent of T is what the authors call k . Another interesting phenomenon already observed in [8] and also present in our setting is mode collapse. This can be clearly seen in the fifth row of Fig. 3-a, where the generated sample at $t = T$ would have been classified as an 8 but later evolves to become a 1. We empirically observe that this also happens with models trained on FashionMNIST, but less frequently.

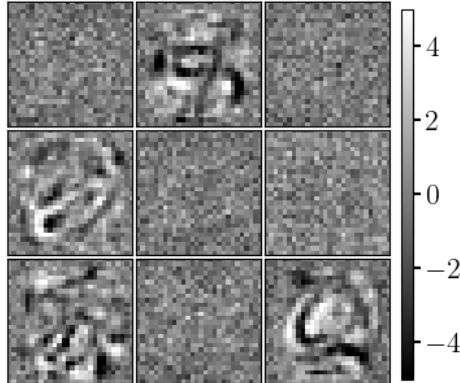


Figure 4. Receptive fields of 9 randomly chosen hidden neurons in the 2-layer Restricted version trained on MNIST. Note that the overall color scale has been divided by g .

Lastly in Fig. 4, we show the receptive fields of hidden neurons of the 2-layer Restricted model trained on MNIST. Specifically, we plot for some indices $a \in [1, N_h]$ the weights $\{W_{ia} + A_{ia}\}_{i=1, \dots, N_v}$ connecting the hidden unit h_a to the visible layer \mathbf{v} . After training, about half of the hidden neurons have spatially structured receptive fields, as is typically the case in trained RBMs [5, 19], while the other half have random receptive fields not much different than their initial state when $A_{ai} = 0$. We suspect that these unstructured connections are important to maintain a certain level of chaos in the dynamics.

IV. CONCLUSIONS

In this work, we investigated the possibility of using high-dimensional chaotic activity to train recurrent dynamical systems as generative models. The resulting models are autonomous, i.e. they do not require an external noise injection. Furthermore, the learning rules are essentially Hebbian, so this perspective could be an interesting starting point towards more biologically plausible generative models.

Our implementation uses vanilla learning rules that are most likely sub-optimal. It would be interesting to see if modifying the learning rules with standard tricks like regularization, momentum or centering of gradients [19, 20] would improve the quality of the generated samples. Another interesting perspective would be to modify the learning rule by applying a non-linear function to the Hebbian terms, as was done in Dense Associative Memory networks [12], to see if this would improve the memory capacity and thus the expressivity of the generative model.

Finally, the study presented here heavily relied on numerical simulations. A theoretical approach to the questions discussed in this manuscript is possible by combining simplified high-dimensional non-linear chaotic systems and dynamical mean field theory [21].

Acknowledgments – Ce travail a bénéficié d’une aide de l’État au titre de France 2030 (PhOM -Graduate School Physique) portant la référence ANR-11-IDEX-0003.

-
- [1] E. T. Jaynes. Information Theory and Statistical Mechanics. *Physical Review*, 106(4):620–630, May 1957. Publisher: American Physical Society.
 - [2] E. T. Jaynes. Information Theory and Statistical Mechanics. II. *Physical Review*, 108(2):171–190, October 1957. Publisher: American Physical Society.
 - [3] Simona Cocco, Christoph Feinauer, Matteo Figliuzzi, Rémi Monasson, and Martin Weigt. Inverse statistical physics of protein sequences: a key issues review. *Reports on Progress in Physics*, 81(3):032601, 2018.

- [4] Pankaj Mehta, Marin Bukov, Ching-Hao Wang, Alexandre G.R. Day, Clint Richardson, Charles K. Fisher, and David J. Schwab. A high-bias, low-variance introduction to Machine Learning for physicists. *Physics Reports*, 810:1–124, May 2019.
- [5] Geoffrey Hinton. ARTICLE Training Products of Experts by Minimizing Contrastive Divergence. *Neural computation*, 14:1771–800, September 2002.
- [6] Tijmen Tieleman. Training restricted Boltzmann machines using approximations to the likelihood gradient. In *Proceedings of the 25th international conference on Machine learning - ICML 2008*, pages 1064–1071, Helsinki, Finland, 2008. ACM Press.
- [7] Erik Nijkamp, Mitch Hill, Song-Chun Zhu, and Ying Nian Wu. Learning Non-Convergent Non-Persistent Short-Run MCMC Toward Energy-Based Model. In *Advances in Neural Information Processing Systems*, volume 32. Curran Associates, Inc., 2019.
- [8] Aurélien Decelle, Cyril Furtlehner, and Beatriz Seoane. Equilibrium and non-equilibrium regimes in the learning of restricted Boltzmann machines*. *Journal of Statistical Mechanics: Theory and Experiment*, 2022(11):114009, November 2022. Publisher: IOP Publishing and SISSA.
- [9] Geoffrey E. Hinton. Deterministic Boltzmann Learning Performs Steepest Descent in Weight-Space. *Neural Computation*, 1(1):143–150, March 1989.
- [10] Haim Sompolinsky, Andrea Crisanti, and Hans-Jurgen Sommers. Chaos in random neural networks. *Physical review letters*, 61(3):259, 1988.
- [11] Paul Smolensky. Information processing in dynamical systems: Foundations of harmony theory. *Parallel Distributed Process*, 1, January 1986.
- [12] Dmitry Krotov and John Hopfield. Large associative memory problem in neurobiology and machine learning. *arXiv preprint arXiv:2008.06996*, 2020.
- [13] Emmy Blumenthal, Jason W Rocks, and Pankaj Mehta. Phase transition to chaos in complex ecosystems with nonreciprocal species-resource interactions. *Physical Review Letters*, 132(12):127401, 2024.
- [14] Yann LeCun. The mnist database of handwritten digits. <http://yann.lecun.com/exdb/mnist/>, 1998.
- [15] Y. Lecun, L. Bottou, Y. Bengio, and P. Haffner. Gradient-based learning applied to document recognition. *Proceedings of the IEEE*, 86(11):2278–2324, November 1998. Conference Name: Proceedings of the IEEE.
- [16] Han Xiao, Kashif Rasul, and Roland Vollgraf. Fashion-MNIST: a Novel Image Dataset for Benchmarking Machine Learning Algorithms, September 2017. arXiv:1708.07747 [cs, stat].
- [17] Ruslan Salakhutdinov and Hugo Larochelle. Efficient Learning of Deep Boltzmann Machines. In *Proceedings of the Thirteenth International Conference on Artificial Intelligence and Statistics*, pages 693–700. JMLR Workshop and Conference Proceedings, March 2010. ISSN: 1938-7228.
- [18] Geoffrey E Hinton and Russ R Salakhutdinov. A Better Way to Pretrain Deep Boltzmann Machines. In *Advances in Neural Information Processing Systems*, volume 25. Curran Associates, Inc., 2012.
- [19] Geoffrey E. Hinton. A Practical Guide to Training Restricted Boltzmann Machines. In Grégoire Montavon, Geneviève B. Orr, and Klaus-Robert Müller, editors, *Neural Networks: Tricks of the Trade*, volume 7700, pages 599–619. Springer Berlin Heidelberg, Berlin, Heidelberg, 2012. Series Title: Lecture Notes in Computer Science.
- [20] Jan Melchior, Asja Fischer, and Laurenz Wiskott. How to Center Deep Boltzmann Machines. *Journal of Machine Learning Research*, 17(99):1–61, 2016.
- [21] Samantha J Fournier and Pierfrancesco Urbani. Statistical physics of learning in high-dimensional chaotic systems. *Journal of Statistical Mechanics: Theory and Experiment*, 2023(11):113301, 2023.
- [22] Alessandra Carbone, Aurélien Decelle, Lorenzo Rosset, and Beatriz Seoane. Fast and Functional Structured Data Generators Rooted in Out-of-Equilibrium Physics, July 2023. arXiv:2307.06797 [cond-mat, q-bio].
- [23] Andrew Yale, Saloni Dash, Ritik Dutta, Isabelle Guyon, Adrien Pavao, and Kristin P. Bennett. Generation and evaluation of privacy preserving synthetic health data. *Neurocomputing*, 416:244–255, November 2020.

Appendix A: Definition of the deep restricted architecture

The dynamical equations of the 3-layer Restricted architecture read

$$\tau \frac{dv_i}{dt} = -v_i + \frac{1}{\sqrt{N_h^{(1)}}} \sum_{a=1}^{N_h^{(1)}} \left(W_{ia}^{(1)} + A_{ia}^{(1)} \right) \phi(h_a^{(1)}) + b_i, \quad (\text{A1})$$

$$\tau \frac{dh_a^{(1)}}{dt} = -h_a^{(1)} + \frac{1}{\sqrt{N_v}} \sum_{i=1}^{N_v} \left(\tilde{W}_{ai}^{(1)} + A_{ai}^{(1)} \right) \phi(v_i) + \frac{1}{\sqrt{N_h^{(2)}}} \sum_{b=1}^{N_h^{(2)}} \left(W_{ab}^{(2)} + A_{ab}^{(2)} \right) \phi(h_b^{(2)}) + c_a, \quad (\text{A2})$$

$$\tau \frac{dh_a^{(2)}}{dt} = -h_a^{(2)} + \frac{1}{\sqrt{N_h^{(1)}}} \sum_{b=1}^{N_h^{(1)}} \left(\tilde{W}_{ab}^{(2)} + A_{ab}^{(2)} \right) \phi(h_b^{(1)}) + d_a, \quad (\text{A3})$$

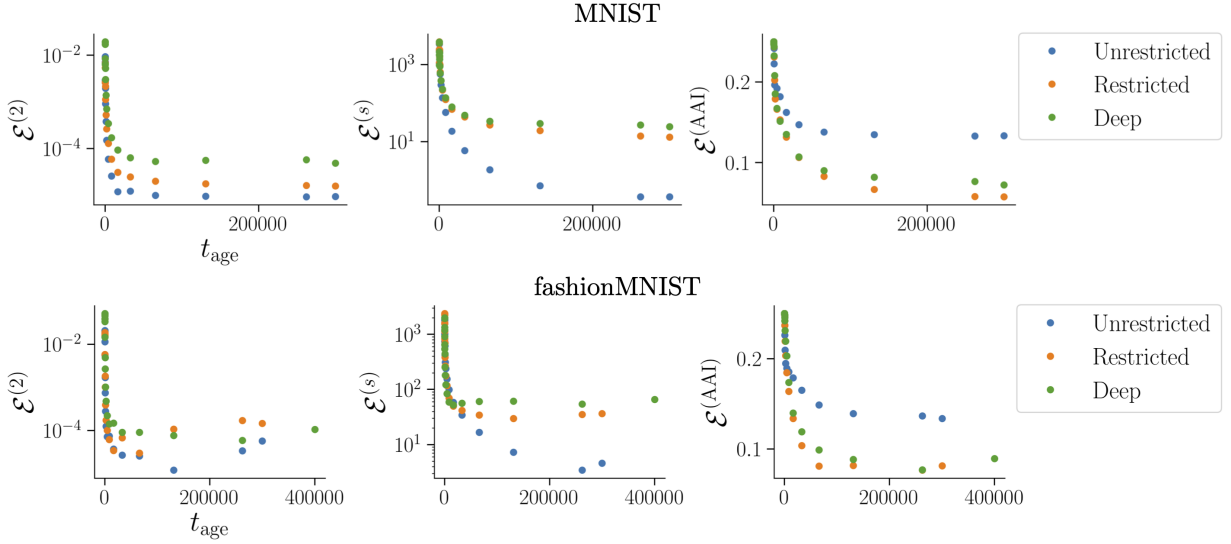


Figure 5. Performance of the different models trained on MNIST (top half) and FashionMNIST (bottom half) during training. The accuracy indicators are computed at the target time $T^* = T$.

where the matrix elements of the connections $W^{(1)}$, $W^{(2)}$, $\tilde{W}^{(1)}$, $\tilde{W}^{(2)}$ are drawn at random from four Gaussian distributions with mean 0 and variance g . The parameters $A^{(1)}$, $A^{(2)}$, \mathbf{b} , \mathbf{c} and \mathbf{d} are initialized at zero and updated at each epoch t_{age} with

$$\Delta A_{ia}^{(1)} = k \left(\langle \xi_i \chi_a^{(1)} \rangle_{\mathcal{D}} - \langle \phi(v_i) \phi(h_a^{(1)}) \rangle_{\mathcal{F}} \right) \quad (\text{A4})$$

$$\Delta A_{ab}^{(2)} = k \left(\langle \chi_a^{(1)} \chi_b^{(2)} \rangle_{\mathcal{D}} - \langle \phi(h_a^{(1)}) \phi(h_b^{(2)}) \rangle_{\mathcal{F}} \right) \quad (\text{A5})$$

$$\Delta b_i = k \left(\langle \xi_i \rangle_{\mathcal{D}} - \langle \phi(v_i) \rangle_{\mathcal{F}} \right) \quad (\text{A6})$$

$$\Delta c_a = k \left(\langle \chi_a^{(1)} \rangle_{\mathcal{D}} - \langle \phi(h_a^{(1)}) \rangle_{\mathcal{F}} \right) \quad (\text{A7})$$

$$\Delta d_a = k \left(\langle \chi_a^{(2)} \rangle_{\mathcal{D}} - \langle \phi(h_a^{(2)}) \rangle_{\mathcal{F}} \right), \quad (\text{A8})$$

where $i = 1, \dots, N_v$, $a = 1, \dots, N_h^{(1)}$ and $b = 1, \dots, N_h^{(2)}$. We call $\{\chi^{(1,\mu)}(T) = \phi(\mathbf{h}^{(1,\mu)}(T))\}_{\mu=1, \dots, M}$ and $\{\chi^{(2,\mu)}(T) = \phi(\mathbf{h}^{(2,\mu)}(T))\}_{\mu=1, \dots, M}$ the samples collected from simulating Eqs. A2-A3 up to time T while the visible units are clamped to a data sample $\phi(\mathbf{v}^{(\mu)})(t) = \boldsymbol{\xi}^{(\mu)}$.

Appendix B: Definition of the accuracy indices

Monitoring the performance of a generative model is not a straightforward task because it is unclear what would be a precise definition of a good generated sample in the case in which the probability distribution of the underlying dataset is unknown. To assess the statistical quality of generated samples, we therefore considered four possible quality measures that were previously studied in the literature [8, 22].

The first one is the error on the second moment $\mathcal{E}^{(2)}$ between the generated and the original datapoints. We define the averaged covariance matrix of the visible units $C_{ij} = \overline{\text{Cov}(\phi(v_i), \phi(v_j))}$ (where $\overline{(\dots)}$ is an average of N_s independent samples). We compute this quantity both on samples from the dataset \mathcal{D} setting $\phi(\mathbf{v}) = \boldsymbol{\xi}$, and on generated samples \mathcal{G} . Here $\mathcal{G} = \{\phi(\mathbf{v}^{(\mu)})(T^*)\}_{\mu=1, \dots, N_s}$ is obtained by running N_s parallel simulations of the free dynamical system up to a target time T^* , starting from a random initialization. We then define $\mathcal{E}^{(2)}$ as the Mean Squared Error (MSE) of their difference:

$$\mathcal{E}^{(2)} = \frac{1}{N_v(N_v - 1)} \sum_{i < j} (C_{ij}^{\mathcal{G}} - C_{ij}^{\mathcal{D}})^2. \quad (\text{B1})$$

The smaller $\mathcal{E}^{(2)}$, the better the statistical distribution of the generated samples.

Next, we define the error on the spectrum $\mathcal{E}^{(s)}$. Let's consider a matrix of samples $X \in \mathbb{R}^{N_s \times N_v}$. Its singular value decomposition (SVD) can be written as $X = USV^T$, where $U \in \mathbb{R}^{N_s \times N_s}$, $V \in \mathbb{R}^{N_v \times N_v}$ and $S = \text{diag}(\{s_\mu\})$, with the singular values s_μ ordered such that $s_1 > s_2 > \dots > s_{N_s}$. These singular values can be computed on a matrix of data samples or of generated samples, so we define $\mathcal{E}^{(s)}$ as

$$\mathcal{E}^{(s)} = \frac{1}{N_s} \sum_{\mu=1}^{N_s} (s_\mu^{\mathcal{G}} - s_\mu^{\mathcal{D}})^2. \quad (\text{B2})$$

For the 2-layer Restricted version of the model, it is also common to look at the so-called reconstruction error $\mathcal{E}^{(R)}$. The idea is to see how well the model can reconstruct a given data sample. To do this, the 2-layer Restricted model is presented with a data sample $\boldsymbol{\xi}^{(\mu)}$ (for $\mu \in \{1, \dots, N_s\}$), from which we compute the activities of the hidden units at time T^* , while the visible units are clamped to the data sample $\phi(\mathbf{v}^{(\mu)}) = \boldsymbol{\xi}^{(\mu)}$. Next, we do the inverse operation: we fix the hidden units to their previously calculated value $\mathbf{h}^{(\mu)}(T^*)$ and predict the activity of the visible units at time T^* . The latter is the generated prediction of the model $\phi(\mathbf{v}^{(\mu)})(T^*)$, which is to be compared with the original data sample $\boldsymbol{\xi}^{(\mu)}$. The reconstruction error is then defined as the MSE of their difference, averaged over visible sites i and independent samples μ :

$$\mathcal{E}^{(R)} = \frac{1}{N_s N_v} \sum_{\mu=1}^{N_s} \sum_{i=1}^{N_v} \left(\xi_i^{(\mu)} - \phi(v_i^{(\mu)}) \right)^2. \quad (\text{B3})$$

Lastly, we define the error on the Adversarial Accuracy Indicator (AAI). This score was originally introduced in [23]. The goal with this indicator is to measure how well data samples and generated samples are mixed with one another. We start by creating a matrix of samples $X \in \mathbb{R}^{2N_s \times N_v}$ by stacking together the data and the generated samples. We then create a matrix D whose entries are the euclidean distance between each pair of samples in X . By taking the minimum of each rows of D , we can compute $P_{\mathcal{G}\mathcal{G}}$ and $P_{\mathcal{D}\mathcal{D}}$ defined respectively as the probability that a generated sample has a nearest neighbor (n.n.) which is also a generated sample, and the probability that a data sample has a n.n. which is also a data sample. If the generated and data samples are perfectly mixed, $P_{\mathcal{G}\mathcal{G}}$ and $P_{\mathcal{D}\mathcal{D}}$ should both be 0.5, so we define $\mathcal{E}^{(AAI)}$ as:

$$\mathcal{E}^{(AAI)} = 0.5 \left[(P_{\mathcal{G}\mathcal{G}} - 0.5)^2 + (P_{\mathcal{D}\mathcal{D}} - 0.5)^2 \right]. \quad (\text{B4})$$

These quality measures are computed over a batch of samples generated from the dynamical system at a target time T^* , which can be equal to T or generic. The behaviour of these accuracy indicators computed from samples generated by a trained model as a function of a generic $T^* = t$ is reported Fig. 3-b. Instead, the behaviour of these accuracy indicators computed from samples generated at $T^* = T$ as a function of the training epoch t_{age} are shown Fig. 5 ($\mathcal{E}^{(R)}$ is not shown). We observe that all the error functions decrease steeply at the beginning of training and then saturate to small values. It is interesting to note that the error functions are not always in agreement with regards to which model architecture performs best. These error functions are therefore just a coarse way of quantifying the performance of a generative model.